

# Chapter 1

## INTRODUCTION

### 1.1 Control of chaotic dynamical systems

Nowadays, the diversity of techniques, perspectives, and kind of problems that chaos control deals with contrasts sharply with classical control tasks such as that of stabilizing an equilibrium state. This is a direct consequence of taking into account two generic properties of real-world dynamical systems: nonlinearity and non-integrability. This book is about control of homoclinic and heteroclinic chaos in nonlinear, non-autonomous and *dissipative*, oscillator systems by weak periodic (mainly harmonic) excitations. It describes a rapidly growing subfield of chaos control with applications to a great number of problems in engineering and science such as fluid mixing, Josephson junction arrays, and secure information processing, to mention only a few. In this monograph control of chaos is understood in the broadest sense: a procedure to enhance or suppress chaos depending upon the needs. Enhancement of chaos means increasing the duration of a chaotic transient, passing from transient to steady chaos, or increasing the leading (positive) Lyapunov exponent of the initial chaotic state. Suppression of chaos means decreasing the duration of a chaotic transient, passing from steady chaos to a regular state via transient chaos or not, or decreasing the positive Lyapunov exponent of the initial chaotic attractor.

Although an exhaustive classification (and discussion) of the different methods of controlling chaos is beyond the purpose of the present work, one can roughly classify them into two kinds: feedback methods and non-feedback methods. Feedback methods inhibit chaos by stabilizing one of the unstable periodic orbits embedded in an existing chaotic attractor by means of weak time-dependent variations of a system parameter. Such control methods are important for two reasons. First, since they are based on fairly generic properties of chaotic dynamics, they are *a priori* applicable to a broad diversity of dynamical systems. Second, since chaotic systems present an infinite number of unstable periodic orbits, a given dynamical system can *a priori* exhibit a broad diversity of controlled responses. On the other hand, since feedback methods involve detection of the degree of deviation of the selected unstable periodic orbit from the chaotic state in real time, the control experimental device typically becomes a closed-loop system, and thus tends to be relatively complicated. Other essential limitations of such methods lie in their inability to control both high-speed chaotic systems (such as Josephson junction arrays or fast electro-optical systems)

and chaotic systems embedded in highly noisy environments. All this limits the scope and applicability of the feedback methods: they become impractical for the control of fast processes and large systems.

## 1.2 Non-feedback control methods

Non-feedback methods suppress or enhance chaos by adding a (preferably) weak time-dependent forcing or by perturbing a system parameter with (preferably) small time-dependent excitations. Periodic signals have been by far the most commonly chosen as control excitations, albeit the study of the effect of random and chaotic time-dependent excitations in controlling chaos has also been initiated. In contrast to the procedure of feedback methods, such control excitations are *independent* of the system's state. This distinctive characteristic presents both advantages and difficulties. On the one hand, the control experimental device is typically a rather simple high-speed open-loop system which does not require on-line monitoring or processing. Thus, non-feedback methods are attractive due to both their easy applicability to experimental situations and their robustness *vis-à-vis* noise. On the other hand, the main criticism of such methods focuses on the difficulty of predicting the nature of the regularized state as well as the parameter ranges for control. This is clearly the case of high-dimensional systems such as solid state lasers and neural network models where the absence of a unified theoretical approach implies a *tentative* application of the control excitations. However, it will be shown in this book that a rigorous control theory is emerging for a certain class of important low-dimensional systems, including the perturbed pendulum as well as other universal models. Such a theory provides analytical estimates of the ranges of parameters of the chaos-controlling excitation for enhancement/suppression of the initial chaos, as well as key information concerning the periodicity of the regularized responses.

Various techniques of non-feedback control have been proposed that can be roughly classified into three types: (i) the parametric excitation of an experimentally adjustable parameter; (ii) entrainment to the target dynamics; (iii) the application of an external periodic excitation. It will be shown in the next chapter that techniques (i) and (iii) may be unified in a general setting for the class of dissipative systems considered in this work. There exists numerical, theoretical, and experimental evidence that the period of the *most effective* chaos-controlling excitations usually is a rational fraction of a *certain* period associated with the uncontrolled system, although the effectiveness of incommensurate excitations has also been demonstrated in some particular cases. Indeed, resonances between the chaos-controlling excitation and (i) a (periodic) chaos-inducing excitation, (ii) an unstable periodic orbit embedded in the chaotic attractor, (iii) a natural period in a period-doubling route to chaos, or (iv) a period associated with some peak in the power spectrum, have been considered in diverse successful chaos-controlling excitations. This is not really surprising since these types of resonances are closely related to each other. For instance, when

a damped, harmonically forced oscillator presents steady chaos, the power spectrum corresponding to a given state variable typically presents its main peaks at frequencies which are rational fractions of the chaos-inducing frequency for certain ranges of the chaos-inducing amplitude.

### 1.3 Controlling chaos by weak periodic excitations

The present book is concerned with the control of chaos in dissipative non-autonomous systems described by the differential equation

$$\ddot{x} + \frac{dU(x)}{dx} = -d(x, \dot{x}) + p_c(x, \dot{x})F_c(t) + p_s(x, \dot{x})F_s(t), \quad (1.1)$$

where  $U(x)$  is a nonlinear potential,  $-d(x, \dot{x})$  is a generic dissipative force which may include constant forces and time-delay terms,  $p_c(x, \dot{x})F_c(t)$  is a chaos-inducing excitation, and  $p_s(x, \dot{x})F_s(t)$  is an as yet undetermined suitable chaos-controlling excitation, with  $F_c(t), F_s(t)$  being harmonic functions of initial phases  $\Theta, \Theta$ , and frequencies  $\omega, \Omega$ , respectively. The theory discussed in Chap. 2 (developed on the basis of Melnikov's method) imposes on Eq. (1.1) some additional limitations: the excitation, time-delay, and dissipation terms are weak perturbations of the underlying conservative system  $\ddot{x} + dU(x)/dx = 0$  which has a separatrix. These restrictions will not apply, however, in discussing the mechanisms underlying the control of chaos by weak periodic excitations in Chap. 3.

#### 1.3.1 Robustness and flexibility

It is shown in Chap. 4 that the theoretical results demonstrated in Chap. 2, concerning periodic chaos-inducing excitations, are also valid for chaotic chaos-inducing excitations whose power spectra exhibit a strong peak at a certain frequency which is taken as the chaos-inducing frequency. A similar effectiveness is found for quasiperiodic chaos-inducing excitations where the existence of two incommensurate strong peaks in the power spectrum increases the complexity of the control scenario. These results represent a new aspect of the robustness in the control of chaos by weak harmonic excitations, which extends the well-known robustness against external noise (both additive and multiplicative), and thus make this control method highly reliable. Another attractive aspect is its flexibility in the choice of particular chaos-controlling excitations. Indeed, the theorems of Chap. 2 do not impose any restriction on the nature of such excitations except their perturbational (small amplitude) character. Depending upon the specific chaotic system to be controlled, the chosen chaos-controlling excitation can be a parametric excitation of a potential term, a parametric excitation of a dissipative term, an (additional) forcing term, a parametric excitation of the (periodic) chaos-inducing signal, and so on. However, it is worth mentioning that the phenomenon of *parametric resonance* diminishes or even completely prevents the control of chaos by *certain* parametric excitations. An illustrative example of this effect appears in the problem of controlling chaotic escape from a potential well (cf. Sec. 4.1).

### 1.3.2 Applicability and scope

The aforementioned *hyper-robustness* of the present control method permits its reliable application to a broad spectrum of experimental realizations. In testing the robustness of the method *vis-à-vis* experiment one must assume that the parameters of the chaos-inducing excitation (amongst others) can be affected by random fluctuations. The theoretical predictions for the suitable amplitudes and initial phases of the chaos-controlling excitation are in the form of *finite* intervals whose widths are typically much larger than the error bars associated with the fluctuations. The frequency is a more delicate parameter since the control theorems require an *exact* resonance condition between the two frequencies involved (chaos-inducing and chaos-controlling). Numerical simulations show that the effect of a slight deviation from the resonance condition is an adiabatic (very slow) variation of the initial phase of the chaos-controlling excitation. Since the ranges of suitable initial phases are real intervals, the “off-resonance” chaos-controlling excitation could yield, at least, an intermittent control of the dynamics.

It should be emphasized that Eq. (1.1), including such paradigmatic dynamical systems as the pendulum and the two-well Duffing oscillator, also appears when modeling key aspects underlying the dynamics of more complex systems like chaotic coupled oscillators and nonlinear wave equations. Thus, the findings of this present book will also apply directly to diverse situations concerning the control of spatio-temporal chaos.

### 1.4 Harmonic versus non-harmonic excitations: the waveform effect

It is clear at first sight from the literature that it is harmonic excitations which have been overwhelmingly chosen as representative of periodic control excitations. Since harmonic functions are solutions of linear differential equations (rarely of nonlinear equations), this means that the role to be played by the excitation’s shape in controlling chaos has not as yet been fully explored. However, there exist theoretical and numerical results in support of the existence of generic routes of order $\leftrightarrow$ chaos by changing only the waveform of a periodic excitation. As will be shown below, such reshaping-induced routes are closely related to those associated with the application of harmonic excitations. As a first example, consider the family of systems

$$\ddot{x} + \frac{dU(x)}{dx} = -d(x, \dot{x}) + F(t), \quad (1.2)$$

where  $U(x)$  is a nonlinear potential,  $-d(x, \dot{x})$  is a general dissipative force, and  $F(t)$  is a general periodic function of period  $T$ . Figure 1.1 shows an illustrative example of an order $\leftrightarrow$ chaos route induced by solely reshaping a periodic excitation, corresponding to a linearly damped pendulum subjected to a periodic string of symmetric pulses:

$$\ddot{x} + \sin x = -\eta\dot{x} + \gamma \operatorname{cn}(\omega t; m), \quad (1.3)$$

where  $\eta, \gamma > 0$ , and  $\text{cn}(\omega t; m)$  is the Jacobian elliptic function of parameter  $m$ . When  $m = 0$ , then  $\text{cn}(\omega t; m = 0) = \cos(\omega t)$ ; i.e., one recovers the well-known case of harmonic forcing. To study the structural stability of the pendulum when only the forcing waveform is varied, one fixes the forcing period  $T = \text{const}$ , making the frequency  $\omega = \omega(m) \equiv 4K(m)/T$ , where  $K$  is the complete elliptic integral of the first kind. Note that, by increasing  $m$ , the pulse becomes narrower and narrower, and for  $m \simeq 1$  one recovers a periodic sharply kicking forcing very close to the periodic two-sided  $\delta$ -function, but with finite width and amplitude as in real-world pulses. Figure 1.1 shows the bifurcation diagram for the variable  $dx/dt$  versus  $m$ , with  $\eta = 0.5, \gamma = 1.1$ , and  $T = 3\pi$ .

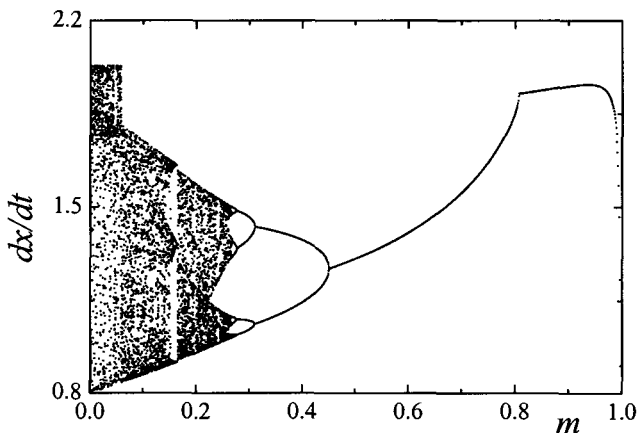


Figure 1.1: Bifurcation diagram corresponding to the pendulum (1.3).

It is worth mentioning that, for fixed  $T, x(0), \dot{x}(0)$ , the same qualitative phenomena seen in this figure continued to be seen as the ratio  $\eta/\gamma$  is varied over a *certain* range (depending upon  $T, x(0), \dot{x}(0)$ ), the difference being the specific values of the waveform parameter  $m$  at which the qualitative changes (crisis, bifurcations, and so on) occur. In particular, the threshold value  $m_{\text{threshold}}$  such that  $\lambda(m \geq m_{\text{threshold}}) \leq 0$  decreases as  $\eta/\gamma$  is increased. Figure 1.2 depicts the leading Lyapunov exponent  $\lambda$  versus the waveform parameter  $m$  for  $T = 3\pi$  and two values of  $\eta/\gamma$ : 0.454545 (■) and 0.166666 (★). In such a situation, assume that the pendulum (1.3) is in a chaotic state for  $\eta/\gamma = (\eta/\gamma)_1$  denoted by A (see Fig. 1.2). Then, increasing  $m$  from  $m_1$  to  $m_2$ , and keeping the ratio  $\eta/\gamma = (\eta/\gamma)_1$  constant, the Lyapunov exponent  $\lambda$  decreases and, in some cases, becomes negative which means that the pendulum reaches a regular (periodic or equilibrium) state (as in the case indicated by point B). Contrariwise, if B represents a periodic state for example, the route B→A makes it chaotic (see Fig. 1.2).

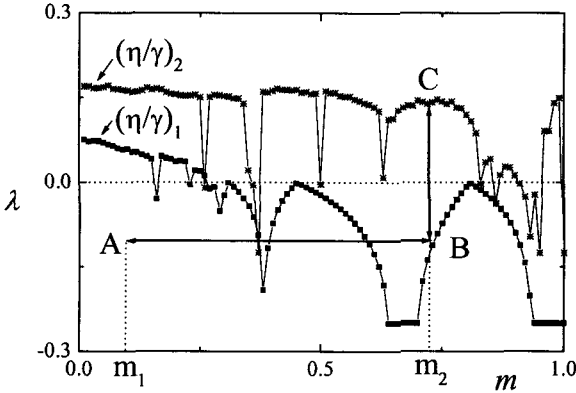


Figure 1.2: Leading Lyapunov exponent vs  $m$  for the pendulum (1.3).

Now, fixing  $m = m_2$  (i.e., fixing the waveform) one can diminish the ratio  $\eta/\gamma$  (raising  $\gamma$ , lowering  $\eta$ , or both) such that the Lyapunov exponent  $\lambda$  increases and, in some case (here for  $\eta/\gamma = (\eta/\gamma)_2$ ), becomes positive, and thus the pendulum reaches a chaotic state (as in the instance indicated by point C). This is a well-known route to reach a chaotic state in non-autonomous systems. Observe that the pathways of types  $A \leftrightarrow B$  and  $C \leftrightarrow B$  are only *ad hoc* routes from chaotic (regular) states to regular (chaotic) states, the most common being a *simultaneous variation* of the excitation waveform and the relative strength of the damping coefficient with respect to the excitation amplitude. This is closely related to the scenario behind the control of chaos by resonant periodic excitations. In particular, this is exactly the case for the family of systems

$$\ddot{x} + \frac{dU(x)}{dx} = -\eta\dot{x} + \gamma \cos(\omega t) + \alpha\gamma \cos(\Omega t + \Theta), \quad (1.4)$$

where  $\alpha\gamma \cos(\Omega t + \Theta)$  is the chaos-controlling excitation ( $0 < \alpha < 1$ ). Indeed, in Eq. (1.4) the resonance between the forcing terms implies  $\Omega/\omega = n/m$ ,  $n, m$  positive integers, i.e., both cosines have a *common* period  $T = 2\pi m/\omega$  and the addition of  $\alpha\gamma \cos(\Omega t + \Theta)$  to  $\gamma \cos(\omega t)$  has the effect of changing both the waveform and the amplitude of the chaos-inducing forcing. Therefore, it is possible that, by choosing suitable values of  $\alpha$  and  $\Theta$  for each resonance  $\Omega/\omega$ , the initial chaotic state may be controlled (i.e., suppressed or enhanced).

#### 1.4.1 Reshaping-induced strange non-chaotic attractors

As a second example, a route by which strange non-chaotic attractors arise and ultimately become chaotic by altering solely the shape (of, for instance, only one periodic term) of a two-period excitation will be characterized in the following.

For the sake of clarity, consider first the reshaping-induced appearance of strange non-chaotic attractors by studying the analyzable two-dimensional map

$$z_{n+1} = [a \operatorname{cn}(\Omega\theta_n; m) + b] \sin z_n, \quad (1.5)$$

$$\theta_{n+1} = (\theta_n + 2\pi\omega) \bmod (2\pi), \quad (1.6)$$

where  $a$  and  $b$  are parameters, and  $\operatorname{cn}(\Omega\theta; m)$  is the Jacobian elliptic function of parameter  $m$ . For irrational  $\omega$ , the circle map (1.6) defines a quasiperiodic excitation which is multiplicative in the nonlinear equation (1.5). Since we are interested in the case when solely the  $\operatorname{cn}$  shape is varied, one fixes its period  $T = \text{const}$ , making  $\Omega = \Omega(m) \equiv 4K(m)/T$ , where  $K(m)$  is the elliptic integral of the first kind. Note that, when  $m = 0$ , then  $\operatorname{cn}[\Omega(m=0)\theta; m=0] = \cos(2\pi\theta/T)$ , i.e., one recovers the well-known harmonic limiting case.

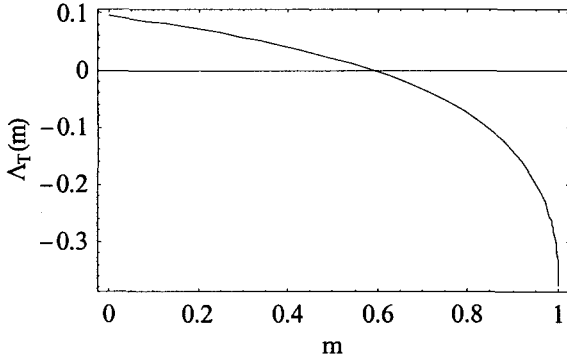


Figure 1.3: Lyapunov exponent  $\Lambda_T(m)$  vs  $m$  for the map (1.5), (1.6).

With increasing  $m$ , the shape of the excitation becomes ever narrower, and for  $m \approx 1$  one has a periodic sharply kicking excitation. In the other limit one has  $\operatorname{cn}[4K(m \rightarrow 1)\theta/T; m \rightarrow 1] = 0$ , i.e., the pulse area tends to 0 if  $m \rightarrow 1$ , for  $T = \text{const}$ , so that the  $z$  and  $\theta$  dynamics decouple in this limit. The nonlinearity in Eq. (1.5) is the same as in its harmonic counterpart, so that one straightforwardly obtains that the one-dimensional invariant subspace is  $z = 0$ , while the transverse Lyapunov exponent (for  $T = 2\pi$ ) is

$$\Lambda_T = \frac{1}{2\pi} \int_0^{2\pi} \operatorname{Ln} \left| a \operatorname{cn} \left[ \frac{2K(m)z}{\pi}; m \right] + b \right| dz. \quad (1.7)$$

For the two limiting values of the shape parameter  $\{0, 1\}$ , one has  $\Lambda_T(m=0) = \operatorname{Ln}|b| - \operatorname{Ln}\{2/\{1 + [1 - (a/b)^2]\}\}$  if  $a \leq b$ ,  $\Lambda_T(m=1) = \operatorname{Ln}|b|$ . With  $a$  and  $b$  constant, one can study the transverse Lyapunov exponent as a function of the excitation

shape parameter  $m$  only. A typical plot of  $\Lambda_T(m)$  is shown in Fig. 1.3. The qualitative form of this function remains the same as  $a$  and  $b$  are varied. Thus, for the case  $a > 2, 1 > b > 0$ , there always exists a critical value  $m = m_c \equiv m_c(a, b)$  such that  $\Lambda_T(m \leq m_c) \geq 0$  (a strange non-chaotic attractor appears) and  $\Lambda_T(m > m_c) < 0$  (the attractor is the line  $z = 0$ ). Figure 1.4 shows a typical sequence of phase portraits illustrating the evolution of strange non-chaotic attractors in phase space as the shape parameter approaches its critical value  $m_c$ , the remaining parameters held constant. It is worth mentioning that the particular form of the curve plotted in Fig. 1.3 is closely related to that of (the reciprocal of) the function  $K(m)$ , which controls the rate at which the excitation waveform is varied in the map (1.5), (1.6). In other words, the specific form of the corresponding curve  $\Lambda_T$  (as a function of a certain *effective* shape parameter) should strongly depend, in a general case, on the particular rate at which the excitation waveform is varied, the amplitude and the period being held constant.

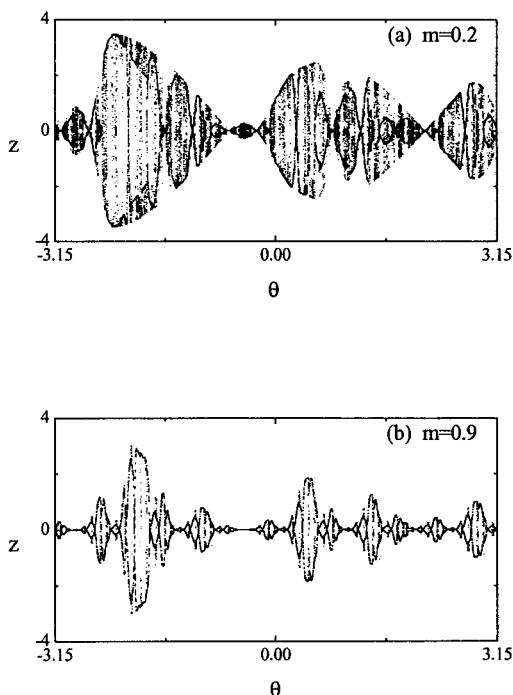


Figure 1.4: Phase portraits corresponding to the map (1.5), (1.6).

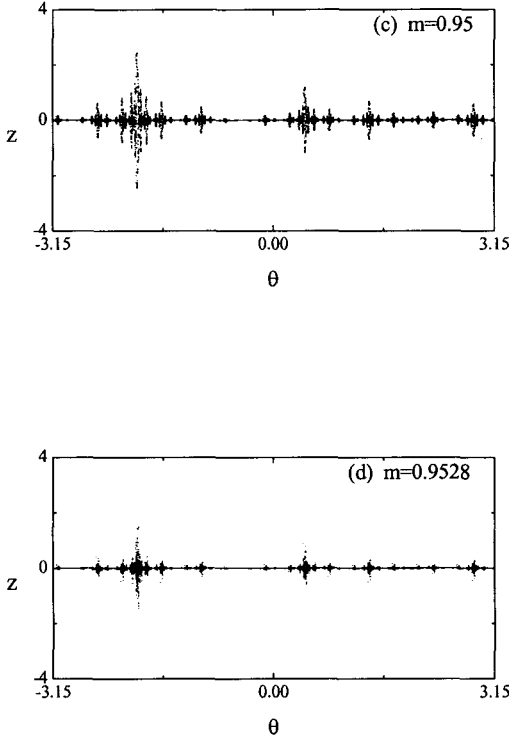


Figure 1.4: (Continued)

For a generic excitation  $f(\theta; T, \alpha_i)$  of period  $T$ , unit amplitude, and shape controlled by parameters  $\alpha_i$ , a physically plausible candidate for such an effective shape parameter  $p_{ef}$  could be the mean value of its absolute value:  $p_{ef} = p_{ef}(\alpha_i) \equiv (1/T) \int_0^T |f(\theta; T, \alpha_i)| d\theta$ . For example, one finds  $p_{ef}(m) = [(1-m)/m]^{1/2} K^{-1}(m)$  for the above elliptic excitation  $cn$ , so that the functions  $-p_{ef}(1-m), \Lambda_T(m)$  have almost identical forms. It is straightforward to see that, when the variation of the (effective) shape parameter is monotonous, there exists a *unique* critical value for the transition to strange non-chaotic attractor (given a suitable choice of the remaining parameters), while for non-monotonous changes one finds (for the same suitable set of the remaining parameters) a number of critical values depending upon the specific variation. As an illustrative example, consider now  $K(g(m))$  instead of  $K(m)$  in the map (1.5), (1.6), where  $g(m) \equiv (32/3)m^3 - 16m^2 + (19/3)m$  is a function with a single maximum and a single minimum. Note that we choose the function  $g = g(m)$ , with  $g(m=0) = 0, g(m=1) = 1$ , and  $0 \leq g(m) \leq 1, m \in [0, 1]$ , in order for the excitation  $cn[2K(g(m))\theta/\pi; m]$  to have the same period ( $2\pi$ ) for all  $m$ .

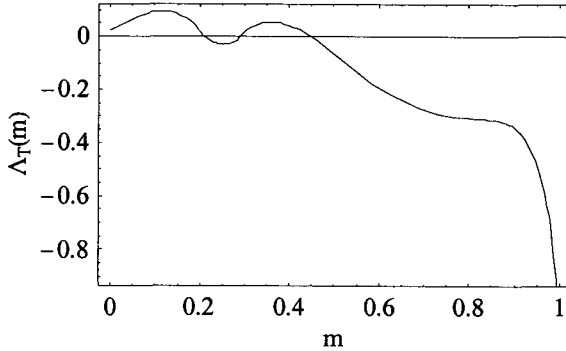


Figure 1.5: Lyapunov exponent  $\Lambda_T(m)$  vs  $m$  for the map (1.5), (1.6).

Figure 1.5 shows the corresponding transverse Lyapunov exponent vs the shape parameter, where one sees three critical values for the appearance (disappearance) of strange non-chaotic attractors. Therefore, the appearance or suppression of strange non-chaotic attractors can be induced, at will, by *suitably reshaping the excitation waveform*.

Consider now an elliptic generalization of the two-period quasiperiodically (using harmonic functions) forced damped pendulum:

$$\ddot{\phi} + \nu \dot{\phi} + \sin \phi = A + V [\text{cn}(\Omega t; m) + \cos(\omega t)], \quad (1.8)$$

where  $\phi$  is the angle of the pendulum with the vertical axis,  $\nu$  is the dissipation coefficient,  $A$  is a constant,  $V$  is the excitation amplitude, and  $\Omega = \Omega(m) \equiv 4K(m)/T_{\text{cn}}$ ,  $\omega = 2\pi/T_{\text{cos}}$ , where  $T_{\text{cn}}$  and  $T_{\text{cos}}$  are two incommensurate periods. After fixing the parameters  $\nu = 0.8270429$ ,  $A = 0.8$ ,  $V = 0.55$ ,  $T_{\text{cn}}/T_{\text{cos}} = (\sqrt{5} - 1)/2$  (the reciprocal of the golden mean),  $T_{\text{cn}} = 5.196464$  (for which there exists a strange non-chaotic attractor at  $m = 0$ ), one increases the shape parameter to study the stability of such attractors. Recall that the word *strange* has the sense that a strange attractor is an attractor which is neither a finite set of points nor is it piecewise differentiable, while the word *chaotic* has the sense that a chaotic attractor is one for which typical orbits have a positive Lyapunov exponent.

Five ranges can be distinguished as  $m$  varies from 0 to 1. Over the first range,  $0 \leq m \lesssim 0.9$ , one only finds strange non-chaotic attractors which are very similar to that at  $m = 0$ . Figure 1.6(a) shows the leading Lyapunov exponent  $\lambda$  (one Lyapunov exponent is always zero for Eq. (1.8)) vs  $m$  over the mentioned range (strange non-chaotic attractor range). To visualize the attractors, the dimensionless variables  $\phi$  and  $\dot{\phi}$  are plotted on the Poincaré surface of the section defined by  $\omega t_n = nT_{\text{cos}}$ ,  $n = 0, 1, \dots$ .

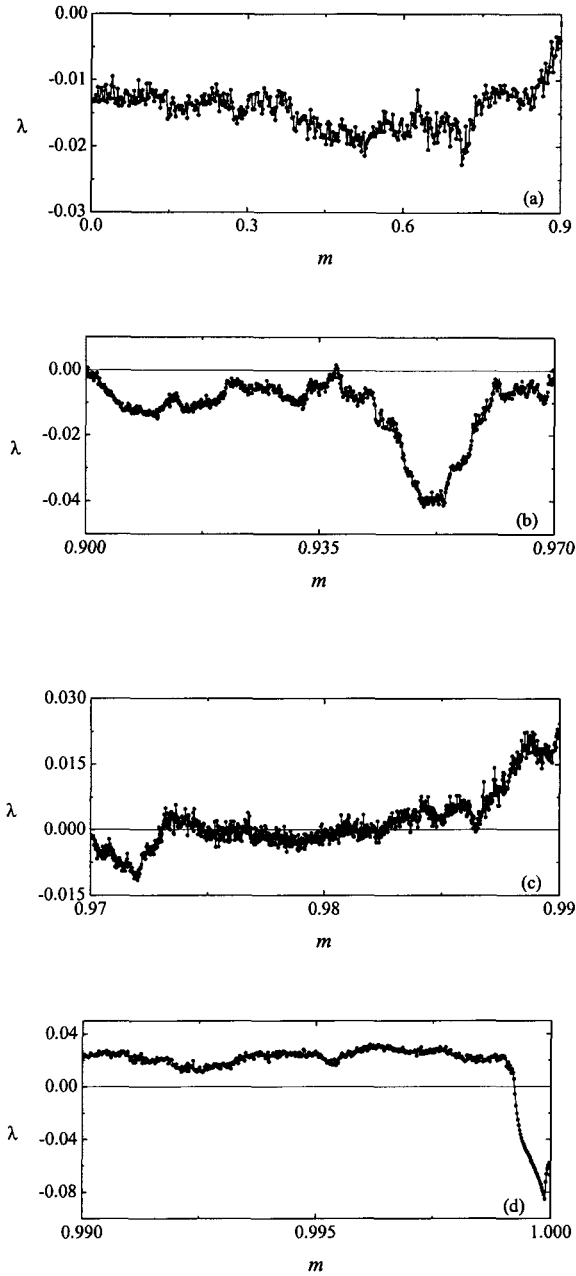


Figure 1.6: The Lyapunov exponent vs the shape parameter for Eq. (1.8).

Figure 1.7(a) shows a single long trajectory on the strange non-chaotic attractor for  $m = 0.017$  ( $\lambda \approx -0.0123$ ) which is typical for the attractors of the strange non-chaotic attractor range.

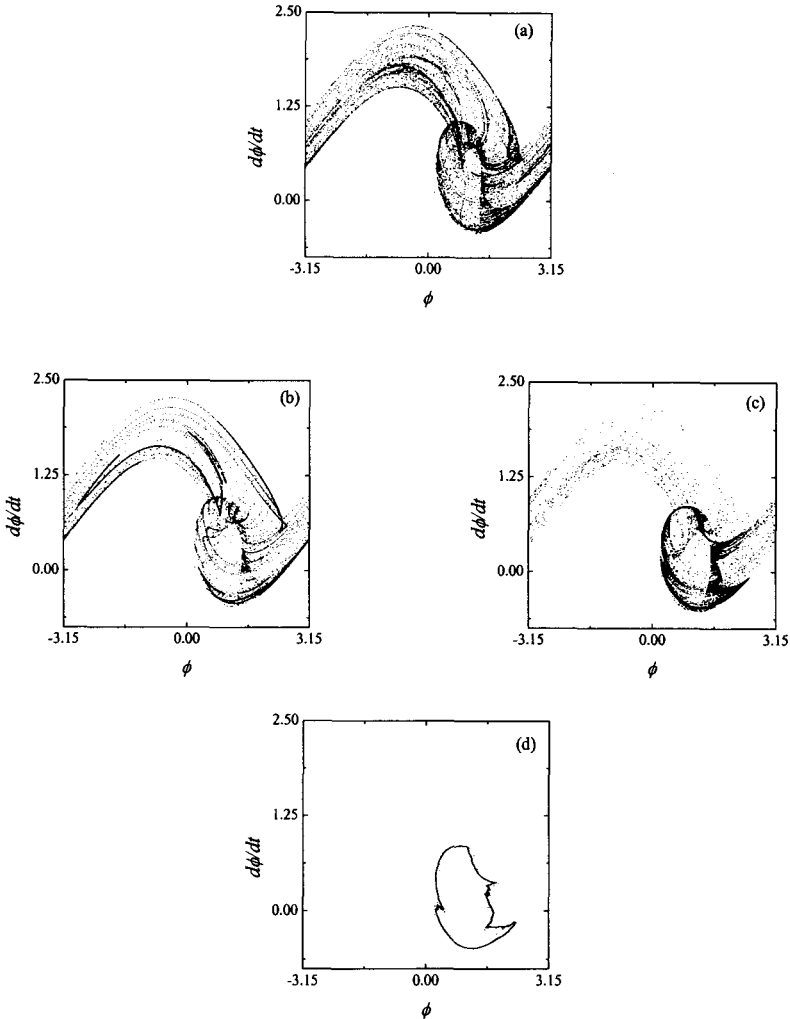


Figure 1.7: Stroboscopic attractors in the  $\phi - \frac{d\phi}{dt}$  plane for the system (1.8).

The next range,  $0.9 \lesssim m \lesssim 0.97$ , is characterized by the overwhelming presence of strange non-chaotic attractors except in a few narrow windows in which chaotic

attractors appear ( $\lambda > 0$ ), as can be seen in Fig. 1.6(b). Note that in this *cohabitation* range the Lyapunov exponent undergoes larger variations than in the preceding range. Figure 1.7(b) gives an example of a strange non-chaotic attractor in the cohabitation range for  $m = 0.951$  (near the minimum,  $\lambda \approx -0.0388$ ). Comparison of Figs. 1.7(a) and 1.7(b) shows how the *strangeness* of the strange non-chaotic attractors varies as the shape parameter changes. Over the range of the transition to chaos,  $0.97 \lesssim m \lesssim 0.99$  (cf. Fig. 1.6(c)), there exist many shape parameter intervals for strange non-chaotic attractors which are interspersed with shape parameter intervals for chaotic attractors. A feature of the central part of this range is that the leading Lyapunov exponent remains very close to zero (the small amplitude fluctuations are artifacts of the numerical computation). Nonetheless, the leading Lyapunov exponent passes through zero *linearly* with respect to the shape parameter near the transition to chaos, thus confirming the scaling behavior found for other control parameters (see Fig. 1.8 where the critical value is  $m_c \approx 0.97309$ ).

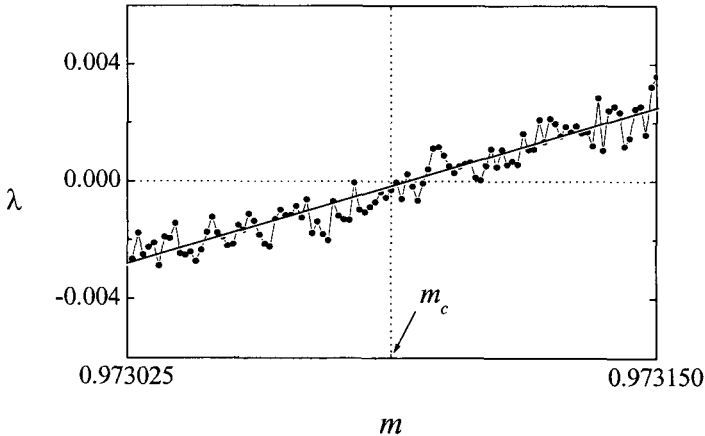


Figure 1.8: The Lyapunov exponent vs the shape parameter for Eq. (1.8).

The fourth range,  $0.99 \lesssim m \lesssim 0.999233$ , is chaotic (see Fig. 1.7(c) for a chaotic attractor at  $m = 0.99923$ ). The final range,  $0.999233 \lesssim m \leq 1$  (cf. Fig. 1.6(d)), is two-frequency quasiperiodic, as in the example depicted in Fig. 1.7(d) at  $m = 0.999235$ . This quasiperiodic range is a consequence of the drastic shrinkage of the pulse width as  $m \rightarrow 1$ . Observe that the leading Lyapunov exponent presents a minimum at  $m \simeq 0.999883$  which is apparently related to the beginning of the appearance of symmetry of the two-frequency quasiperiodic attractor. It is worth mentioning that similar results were found for other parameter values.

In conclusion, it was shown that there typically exists a wide range of the shape parameter in quasiperiodically driven dynamical systems where only strange, chaotic and non-chaotic, attractors appear, so that certain control tasks, such as switching

between the two types of strange attractor, can be more easily performed than for other control parameters.

#### 1.4.2 Reshaping-induced crisis phenomena

As a third example, a route by which crises occur by hump-doubling of a parametric excitation which is initially formed by a periodic string of single-humped symmetric pulses will be characterized in the following by studying the analyzable two-dimensional map

$$z_{n+1} = \alpha z_n + z_n^2 + \gamma N(m) \operatorname{sn}(\Omega\theta_n + \Phi; m) \operatorname{dn}(\Omega\theta_n + \Phi; m), \quad (1.9)$$

$$\theta_{n+1} = 2\theta_n \bmod (2\pi), \quad (1.10)$$

where  $\alpha, \gamma, \Omega \equiv 4K(m)/T$ , and  $\Phi \equiv 4K(m)\varphi/T$  ( $\varphi \in [0, T]$ ) are parameters,  $\operatorname{sn}(\cdot; m)$  and  $\operatorname{dn}(\cdot; m)$  are Jacobian elliptic functions of parameter  $m$  ( $K(m)$  is the complete elliptic integral of the first kind), and  $N(m)$  is a normalization function (Boltzmann form),

$$N(m) \equiv \{a + b[1 + \exp((m - c)/d)]^{-1}\}^{-1}, \quad (1.11)$$

with  $a \simeq 0.43932, b \simeq 0.69796, c \simeq 0.3727, d \simeq 0.26883$ , which is introduced for the excitation function to have the same amplitude,  $\gamma$ , and period,  $T$ , for any waveform (i.e.,  $\forall m \in [0, 1]$ ). The excitation function  $p(\theta; m, T) \equiv N(m) \operatorname{sn}(\Omega\theta; m) \operatorname{dn}(\Omega\theta; m)$  is used as an example to illustrate the crisis induced by hump-doubling. One has  $p(\theta; m = 0, T) = \sin(2\pi\theta/T)$ , i.e., one recovers the widely studied case of a single-humped (harmonic) excitation. This is relevant to comparing the structural stability of the map when solely the excitation shape is varied from a single-humped to a double-humped shape. Since  $\operatorname{dn}(\Omega\theta; m)$  represents a periodic string of asymmetric pulses, whose effective width decreases as  $m$  increases from  $m = 0$ , at the limiting value  $m = 1$  the excitation function  $p(\theta; m = 1, T)$  vanishes except on a set of instants that has Lebesgue measure zero, i.e. the variables  $z$  and  $\theta$  decouple.

Numerical simulations indicated that, for certain parameter values, the map (1.9),(1.10) presents two attractors:  $z = \infty$  (which, for the present purposes, should be regarded as a generic non-chaotic attractor) and a chaotic attractor located in the region  $z \in [-0.1, 0.1]$ . By looking at the fixed points of Eqs. (1.9) and (1.10), one deduces the critical parameter values ( $\alpha_c, \gamma_c, T_c, \varphi_c, m_c$ ) for which the two fixed points  $(z, \theta) = \{(z_{ca}, 0), (z_{bb}, 0)\}$  touch (i.e., a crisis occurs), where  $z_{bb}$  is the smallest  $z$  value on the upper ( $z > 0$ ) basin boundary of the attractor  $z = \infty$  while  $z_{ca}$  is the largest  $z$  value on the chaotic attractor. Setting  $\theta = 0$  in (1.9) and assuming that  $z_n$  is independent of  $n$ , one has

$$z_{\pm} = \left\{ 1 - \alpha \pm [(1 - \alpha)^2 - 4\gamma N(m) \operatorname{sn}(4K\varphi/T; m) \operatorname{dn}(4K\varphi/T; m)]^{1/2} \right\} / 2,$$

and  $z_{bb} = z_+, z_{ca} = z_-$ . Therefore, a crisis occurs when  $z_+ = z_-$ , i.e., for

$$\alpha = \alpha_c \equiv 1 - 2 \{ \gamma_c N(m_c) \operatorname{sn}[4K(m_c)\varphi_c/T_c; m_c] \operatorname{dn}[4K(m_c)\varphi_c/T_c; m_c] \}^{1/2}. \quad (1.12)$$

Let us suppose that for fixed  $\gamma \equiv \gamma_c, T \equiv T_c$ , and  $\varphi \equiv \varphi_c (> 0)$ , and  $m \gtrsim 0$  (nearly harmonic excitation), one has that the chosen  $\alpha > \alpha_c = \alpha_c(m)$ . As  $m$  is increased from  $m \gtrsim 0$ ,  $\alpha_c(m)$  increases so that the two fixed points move towards each other and, in some case that depends upon the choice  $(\gamma_c, T_c, \varphi_c, \alpha)$ , coalesce at  $m = m_c$  for which  $\alpha_c(m = m_c) = \alpha$ . Thus, a reshaping induced crisis occurs.

### 1.4.3 Reshaping-induced basin boundary fractality

As a fourth example, a generic route is described for the modification of fractal basin boundaries in nonlinear systems by changing only the shape of a periodic term in the dynamics equations. To demonstrate the new mechanism in the simplest possible context, consider the following two-dimensional map:

$$z_{n+1} = \lambda z_n + \text{cn} \left[ \frac{4K(m)}{\pi} \theta_n; m \right], \quad (1.13)$$

$$\theta_{n+1} = \frac{4K(m)}{\pi} \theta_n \bmod 2\pi, \quad (1.14)$$

where one assumes  $1 < \lambda < 2, 0 \leq \theta < 2\pi, m \in [0, 1]$ , and where  $\text{cn}$  is the Jacobian elliptic function of parameter  $m$  and (real) period  $4K(m)$ , with  $K(m)$  the complete elliptic integral of the first kind. When  $m = 0$ , then  $\text{cn}[4K(m=0)\theta/\pi; m=0] = \cos(2\theta)$ . Increasing  $m$  makes the pulse given by  $\text{cn}[4K(m)\theta/\pi; m]$  progressively narrower. The Jacobian matrix of the map (1.13),(1.14) has eigenvalues  $4K(m)/\pi$  and  $\lambda$  which are greater than 1 so that there can be no attractors with finite  $z$ . In fact, there exist only two attractors ( $z = \infty$  and  $z = -\infty$ ) and one wishes to characterize the evolution of the fractality of their basin boundary,  $z = f(\theta)$ , as  $m$  varies over the range  $[0, 1[$ . To find this boundary set, one notes first that  $\theta_n = [4K(m)/\pi]^n \theta_0 \bmod (2\pi)$ . The map (1.13),(1.14) is two-to-one, i.e., given  $\theta_{n+1}$ , it is not possible to find  $\theta_n$  uniquely since there are two possible solutions of (1.14),

$$\theta_n = \theta_{n+1} / [4K(m)/\pi]$$

and

$$\theta_n = \pi^2 / 2K(m) + \theta_{n+1} / [4K(m)/\pi].$$

However, one can select any  $z_n$  and find one orbit that ends at  $(z_N, \theta_N)$  by using the above  $\theta_n$  and taking

$$z_{n-1} = \lambda^{-1} z_n - \lambda^{-1} \text{cn} \{ [4K(m)/\pi]^n \theta_0; m \}.$$

For the given  $(z_N, \theta_0)$  one finds that this orbit started at

$$z_0 = \lambda^{-N} z_N - \sum_{i=1}^N \lambda^{-i} \text{cn} \left\{ [4K(m)/\pi]^i \theta_0; m \right\}.$$

The boundary between the two basins are those  $(z_0, \theta_0)$  such that  $z_N$  is finite as  $N \rightarrow \infty$ , so these  $z$  and  $\theta$  are related by

$$z = - \sum_{n=1}^{\infty} \lambda^{-n} \operatorname{cn} \left\{ \left[ \frac{4K(m)}{\pi} \right]^n \theta; m \right\} \equiv f(\theta). \quad (1.15)$$

Since  $\lambda > 1$  and  $m \in [0, 1[$ , this sum converges absolutely and uniformly. One also has

$$\frac{df(\theta)}{d\theta} = \sum_{n=1}^{\infty} \left[ \frac{4K(m)}{\pi\lambda} \right]^n \operatorname{sn} \left\{ \left[ \frac{4K(m)}{\pi} \right]^n \theta; m \right\} \operatorname{dn} \left\{ \left[ \frac{4K(m)}{\pi} \right]^n \theta; m \right\}, \quad (1.16)$$

where  $\operatorname{dn}$  and  $\operatorname{sn}$  are the Jacobian elliptic functions. The latter sum diverges  $\forall m \in [0, 1[$  because  $\lambda < 2$ . Hence  $f(\theta)$  is non-differentiable. Figure 1.9 shows approximate plots of the curve (1.15) for three values of the shape parameter  $m = \{0, 0.5, 0.99\}$ . It can be shown that the box-counting dimension of the curve (1.15) is

$$d = d(m) \equiv 2 - \frac{\ln \lambda}{\ln [4K(m)/\pi]}. \quad (1.17)$$

For  $m = 0$ , one recovers the value  $d(m = 0) = 2 - (\ln \lambda) (\ln 2)^{-1}$ , while one obtains  $d(m \rightarrow 1) = 2$  as the symmetric pulses modeled by the function  $\operatorname{cn}[4K(m)\theta/\pi; m]$  become narrow. Figure 1.10 shows the normalized box-counting dimension  $d(m)/d(0)$  versus  $m$  for  $\lambda = \text{const}$ . One sees that the increase in the normalized box-counting dimension is especially noticeable for very narrow pulses ( $m \lesssim 1$ ), which is a consequence of its dependence on  $K(m)$ . It is worth mentioning that similar results can be obtained for other periodic functions instead of  $\operatorname{cn}$  and for other general systems, i.e., the fractality of a basin boundary can be varied by reshaping a suitable periodic term in the dynamics equations.

#### 1.4.4 Reshaping-induced escape from a potential well

As a fifth example, the reshaping-induced chaotic escape of a damped oscillator excited by a periodic string of symmetric pulses of finite width and amplitude from a cubic potential well that typically models a metastable system close to a fold is described. Consider the chaotic escape of the following universal model

$$\ddot{x} + x - \beta x^2 = -\beta \dot{x} + \gamma N(m) \operatorname{sn}[\Phi(t); m] \operatorname{dn}[\Phi(t); m], \quad (1.18)$$

when only the excitation shape is varied from single-humped to double-humped. Here  $\Phi(t) \equiv 4K(m)t/T$ ,  $\operatorname{sn}(\cdot; m)$  and  $\operatorname{dn}(\cdot; m)$  are Jacobian elliptic functions of parameter  $m$  ( $K(m)$  is the complete elliptic integral of the first kind), and  $N(m)$  is given by Eq. (1.11) with the aforementioned meaning.

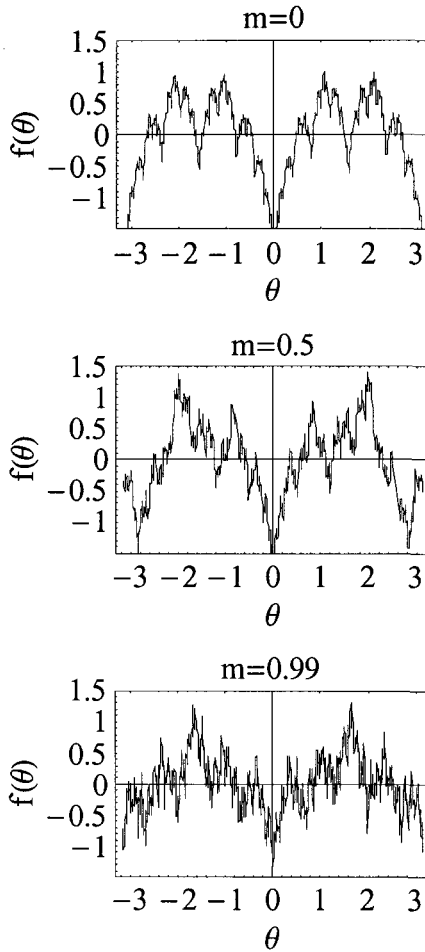


Figure 1.9: Plots of the curve (1.15) for three  $m$  values.

For the universal escape model (1.18), the initial conditions will determine, for a fixed set of its parameters, whether the system escapes to an attractor at infinity, or settles into a bounded oscillation. As is well known, there can exist a rapid and dramatic erosion of the safe basin (union of the basins of the bounded attractors) due to encroachment by the basin of the attractor at infinity (escaping basin). Numerically, one finds that the erosion of the safe basin is maximal as a single-humped excitation transforms into a double-humped excitation, the remaining parameters being held constant.

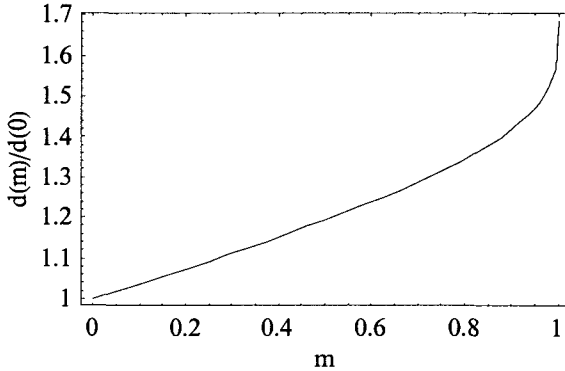


Figure 1.10: Normalized box-counting dimension  $d(m)/d(0)$  vs  $m$  (cf. Eq. (1.17)).

To generate the basins of attraction numerically, a grid of (uniformly distributed)  $300 \times 300$  starting points in the region of phase space  $x(t=0) \in [-0.7, 1.3]$ ,  $\dot{x}(t=0) \in [-0.8, 0.7]$  was selected. From this grid of initial conditions, each integration is continued until either  $x$  exceeds 20, at which point the system is deemed to have escaped (i.e., to the attractor at infinity), or the maximum allowable number of cycles, here 20, is reached. In the case of a single-humped harmonic excitation ( $m=0$ ), one assumes that the system presents a very slight erosion of the non-escaping basin. For a fixed set of parameters  $(\beta, \delta, \gamma, T)$ , the escape probability normalized to that of the case with  $m=0$ ,  $P(m)/P(m=0)$  was calculated. An illustrative example is shown in Fig. 1.11 for the parameters  $\beta=1, \delta=0.1, T=2\pi/0.85$ , and three  $\gamma$  values: 0.071 (circles), 0.072 (triangles), and 0.073 (stars). One sees that the normalized escape probability presents a maximum at  $m_{\max} \simeq 0.65$ . Figure 1.12 shows the corresponding basin erosion sequence for six  $m$  values. The white region represents the non-escaping basin and the black region the escaping basin. One sees that the erosion and stratification of the basin is maximal at  $m \simeq m_{\max}$ .

In order to physically explain the origin of the aforementioned maxima, the impulse transmitted by the excitation over a fixed half-period as a function of the shape parameter is calculated:

$$I(m, T) \equiv \int_0^{T/2} N(m) \operatorname{sn}[\Phi(t); m] \operatorname{dn}[\Phi(t); m] dt = \frac{TN(m)}{2K(m)}. \quad (1.19)$$

One finds that  $I(m, T)$  presents (for each  $T$  value) an absolute maximum at  $m = m'_{\max} \simeq 0.71718$ , which is significantly near the maximum of the normalized escape probability  $m_{\max} \simeq 0.65$ .

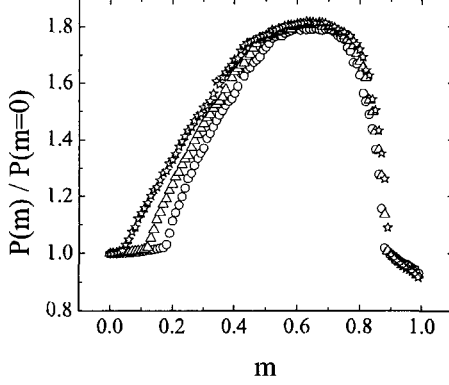


Figure 1.11: Normalized escape probability vs shape parameter.

One can understand such a coincidence by analysing the variation of the system's energy. Indeed, note that Eq. (1.18) can be put into the form,

$$\frac{dE}{dt} = -\delta \dot{x}^2(t) + \gamma \dot{x}(t) N(m) \operatorname{sn}[\Phi(t); m] \operatorname{dn}[\Phi(t); m], \quad (1.20)$$

where  $E(t) \equiv \frac{1}{2}\dot{x}^2(t) + U[x(t)]$  [ $U(x) \equiv \frac{1}{2}x^2 - \frac{1}{3}\beta x^3$ ] is the energy function. Integration of Eq. (1.20) over any interval  $[nT, nT + T/2]$ ,  $n = 0, 1, 2, \dots$ , yields

$$\begin{aligned} \Delta E &= -\delta \int_{nT}^{nT+T/2} \dot{x}^2(t) dt \\ &+ \gamma \int_{nT}^{nT+T/2} \dot{x}(t) N(m) \operatorname{sn}[\Phi(t); m] \operatorname{dn}[\Phi(t); m] dt, \end{aligned} \quad (1.21)$$

where  $\Delta E \equiv E(nT + T/2) - E(nT)$ . Now, if one considers fixing the parameters  $(\beta, \delta, \gamma, T)$  for the system to lie on a periodic orbit (i.e., inside the well) near the underlying separatrix at  $m = 0$ , the application of the first mean value theorem to the second integral on the r.h.s. of Eq. (1.21) gives

$$\Delta E = -\delta \int_{nT}^{nT+T/2} \dot{x}^2(t) dt + \gamma T \dot{x}(t^*) \frac{N(m)}{2K(m)}, \quad (1.22)$$

where  $t^* \in [nT, nT + T/2]$ . Since we are considering that the initial state is a steady (periodic) state,  $t^*$  will depend solely on the excitation function but not on  $n$ . In this situation, one increases  $m$  while holding the remaining parameters constant. For values  $m > 0$  such that the system state is still a periodic orbit (which will be necessarily near the initial periodic orbit in the phase space), one expects that both the dissipation work (integral in Eq. (1.22)) and  $\dot{x}(t^*)$  will maintain approximately their

initial values (at  $m = 0$ ) while the impulse  $I(m, T)$  will rise from its initial value, so that, in some case depending upon the remaining parameters, the energy increment  $\Delta E$  could be enough to surpass the threshold escape energy, i.e., the threshold oscillation amplitude to allow escape from the potential well. Clearly, the probability of this event is maximal at  $m = m'_{\max}$  where  $I(m, T)$  presents an absolute maximum, which explains that  $m_{\max} \simeq m'_{\max}$ . For fixed  $\beta, \delta$ , and  $\gamma$ , since the transmitted impulse depends on both the shape parameter and the period, its critical value yielding the aforementioned escape event can in some case be reached at  $m \neq m'_{\max}$  provided that  $T$  is sufficiently large according to Eq. (1.19).

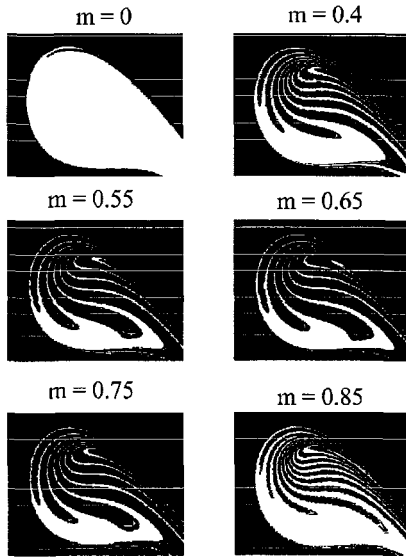


Figure 1.12: Basin erosion sequence for six  $m$  values.

#### 1.4.5 Reshaping-induced control of directed transport

As a sixth example, consider the control of directed transport in general systems. Originally motivated by stochastic models of biomolecular (Brownian) motors, the idea of rectifying transport with the aid of fluctuations has also been discussed in other contexts such as voltages in Josephson junction coupled systems and electrical currents in superlattices. It is worth mentioning that the fluctuations have zero mean value, i.e., the dc component is absent. A fundamental result is that there exists

a clear relationship between directed transport and broken space-time symmetries, which has been generalized from one-particle models to the case of interacting many-particles models. An important consequence is that the symmetries may be broken either by violating the temporal shift symmetry of the ac force or by violating the selection symmetry of the potential in space. Consider a general system (classical or quantum, dissipative or non-dissipative, uni- or multidimensional, noisy or noiseless) where the so-called *ratchet* effect is induced by solely violating temporal symmetries of a  $T$ -periodic zero-mean ac force  $f(t)$  which drives the system. A popular choice would be the simple case of a biharmonic force,

$$f(t) = \epsilon_1 \text{har}_1(\omega_1 t + \varphi_1) + \epsilon_2 \text{har}_2(\omega_2 t + \varphi_2), \quad (1.23)$$

where  $\text{har}_{1,2}$  represents indistinctly sin or cos, and  $p\omega_1 = q\omega_2$ ,  $p, q$  coprime integers. In this case, the aforementioned symmetries are the shift symmetry

$$\mathbf{S}_s : f(t) = -f(t + T/2), \quad (1.24)$$

with  $T \equiv qT_1 = pT_2$  ( $T_i \equiv 2\pi/\omega_i$ ), and the time-reversal symmetries

$$\mathbf{S}_{tr,\pm} : f(-t) = \pm f(t). \quad (1.25)$$

Now the general unsolved problem is to find the regions of the parameter space  $(\epsilon_i, \omega_i, \varphi_i)$  where the ratchet effect is optimal in the sense that the average of relevant observables is maximal, the remaining parameters being held constant. It is shown in the following that such regions are those where the *effective* degree of symmetry breaking is maximal. Without loss of generality, this degree of symmetry breaking mechanism is discussed by using the following working model for the driving force:

$$f_{\text{ellip}}(t) = \epsilon f(t; T, m, \theta) \equiv \epsilon \text{sn}(\Omega t + \Theta; m) \text{cn}(\Omega t + \Theta), \quad (1.26)$$

where  $\text{cn}(\cdot; m)$  and  $\text{sn}(\cdot; m)$  are Jacobian elliptic functions of parameter  $m$ ,  $\Omega \equiv 2K(m)/T$ ,  $\Theta \equiv K(m)\theta/\pi$ ,  $K(m)$  is the complete elliptic integral of the first kind,  $T$  is the period of the force, and  $\theta$  is the (normalized) initial phase ( $\theta \in [0, 2\pi]$ ). Fixing  $\epsilon, T$ , and  $\theta$ , the force waveform changes as the shape parameter  $m$  varies from 0 to 1, as can be appreciated in Fig. 1.13 for  $\epsilon = 1, \theta = 0$ , and three shape parameter values:  $m = 0, 1 - 10^{-6}$  (gray), and 0.96 (black). Note the increasing symmetry-breaking sequence as the pulse narrows, i.e., as  $m \rightarrow 1$ .

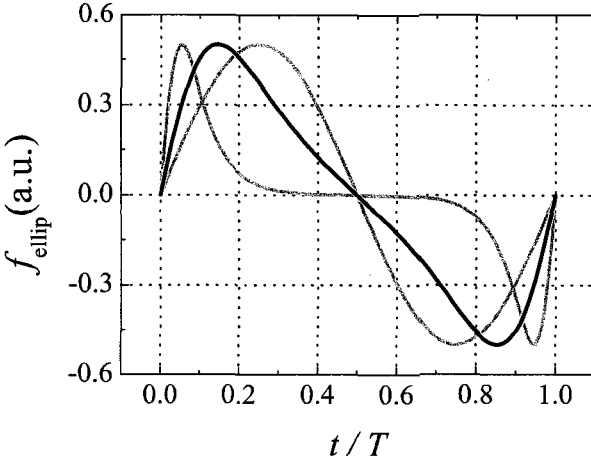


Figure 1.13: Force  $f_{\text{ellip}}(t)$  (Eq. (1.26)) for  $m = 0, 1 - 10^{-6}$  (gray) and 0.96 (black).

Physically, the motivation of choice (1.26) is that  $f(t; T, m = 0, \theta) = \sin(2\pi t/T + \theta)/2$ , and that  $f(t; T, m = 1, \theta)$  vanishes except on a set of instants that has Lebesgue measure zero, i.e., in these two limits directed transport is not possible, while it is expected for  $0 < m < 1$ . Thus, one may expect in general the average of any relevant observable  $\mathfrak{R}$  to exhibit an extremum at a certain value  $m = m_e$  as the shape parameter  $m$  is varied, the remaining parameters being held constant. Clearly, two competing fundamental mechanisms allow one to understand the appearance of such an extremum: the increase of the degree of breaking of the shift symmetry as  $m$  is increased, which increases the absolute value of the average, and the effective narrowing of the force pulse as  $m$  is increased, which decreases the absolute value of the average. The former mechanism arises from the fact that a broken symmetry is a structurally stable situation (Curie's principle) and can be quantitatively characterized by noting that

$$\frac{-f(t + T/2; T, m, \theta)}{f(t; T, m, \theta)} = \frac{\sqrt{1 - m}}{\text{dn}^2(\Omega t + \Theta; m)} \equiv D(t; T, m, \theta), \quad (1.27)$$

where  $\text{dn}(\cdot; m)$  is the Jacobian elliptic function of parameter  $m$ . Equation (1.27) indicates that the degree of deviation from the shift symmetry condition ( $D(t; T, m, \theta) \equiv 1$ ) increases as  $m \rightarrow 1$ , irrespective of the values of the *amplitude*, *period* and *initial phase*. A plot of the asymmetry function  $D(t; T, m, \theta = 0)$  is shown in Fig. 1.14. Thus, while increasing the shape parameter  $m$  ( $0 < m < m_e$ ) improves the directed transport yielding a higher average, it simultaneously narrows the pulse force (see Fig. 1.13), lowering the driving effectiveness of the force. Indeed, the latter becomes the dominant effect for sufficiently narrow pulses ( $m > m_e$ ). Also, one chooses the function (1.26) to satisfy the requirement that  $m_e$  be sufficiently far from 1 for the

elliptic force to be effectively approximated by its first two harmonics. One thus obtains a relationship between the amplitudes of the two harmonics in parametric form:  $\epsilon_{1,2} = \epsilon_{1,2}(m)$ . This relationship does not depend on the initial phase  $\theta$ , and hence neither does it depend on the breaking of time-reversal symmetries of the biharmonic approximation corresponding to the elliptic force.

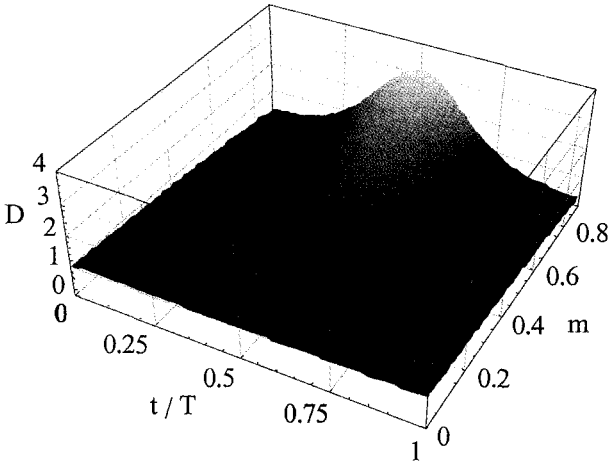


Figure 1.14: Deviation function  $D(t; T, m, \theta = 0)$  (Eq. (1.27)).

For a general biharmonic force (1.23), this means according to the degree of symmetry breaking mechanism that the relationship  $\epsilon_2 = \epsilon_2(\epsilon_1; p, q)$  should control solely the degree of breaking of the shift symmetry. Note that this symmetry is *not* broken when  $p, q$  are both odd integers. Consequently, if the degree of symmetry breaking mechanism is right, the relationship  $\epsilon_2 = \epsilon_2(\epsilon_1; p, q)$  ( $p + q = 2n + 1, n = 0, 1, \dots$ ) controlling the degree of breaking of the shift symmetry should be independent of whichever is the particular system where directed transport is induced. This implies that any averaged observable  $\langle \mathfrak{R} \rangle$  should be proportional to certain function  $g(\epsilon_1, \epsilon_2) \equiv g(\epsilon_1, \epsilon_2; p, q)$  which is  $\sim p_1(\epsilon_1)p_2(\epsilon_2)$  in leading order, with  $p_1(\epsilon_1) \sim \epsilon_1^r, p_2(\epsilon_2) \sim \epsilon_2^s, r, s$  positive integers. Since the aforementioned extremum  $m_e$  is scale-independent, one defines  $\epsilon_1 = \epsilon(1 - \alpha), \epsilon_2 = \epsilon\alpha$  ( $\alpha \in [0, 1]$ ), so that  $g(\epsilon_1, \epsilon_2) \sim (1 - \alpha)^r \alpha^s$  taking  $\epsilon = 1$  without loss of generality. Since the extremum  $m_e$  is independent of the driving period, one has the symmetry relationship  $g(\epsilon_1, \epsilon_2; p, q) = g(\epsilon_2, \epsilon_1; q, p)$ . The problem thus reduces to finding the relationship between  $(r, s)$  and  $(p, q)$ . From Maclaurin's series, one straightforwardly obtains that the *only* function satisfying all these requirements in leading order is  $(1 - \alpha)^p \alpha^q$ , and hence  $g(\epsilon_1, \epsilon_2; p, q) \sim \epsilon_1^p \epsilon_2^q$ . Indeed, previous theoretical analyses of every kind on a great diversity of systems have found that the averaged observable is always proportional to such a factor in leading order. One

thus obtains

$$\langle \mathfrak{R} \rangle \sim \epsilon^3 S(m) \equiv \epsilon^3 \frac{\operatorname{sech}^2 \left[ \frac{\pi K(1-m)}{K(m)} \right] \operatorname{sech} \left[ \frac{2\pi K(1-m)}{K(m)} \right]}{m^3 K^6(m)}, \quad (1.28)$$

for the biharmonic approximation corresponding to the elliptic force (i.e.,  $p = 2, q = 1$ ). Therefore, the shape function  $S(m)$  is a universal function which controls the breaking of the shift symmetry in leading order for the resonance  $(p, q) = (2, 1)$ . It presents a single maximum at  $m = 0.960057 \simeq m_e$  for which  $\epsilon_2 = \epsilon_2(\epsilon_1) = 0.396504\epsilon_1$  (note that  $\epsilon_2 = \epsilon_1/2$  for  $m = 0.983417$ ; see Fig. 1.15). Since the ratchet effect is scale-independent, the critical value  $m_e$  could well be defined by a purely geometric condition which takes into account the two aforementioned competing mechanisms (degree of symmetry breaking and narrowing of the force pulse):  $A(m = m_e)/A(m = 0) = \Phi/2$ , where  $\Phi = (\sqrt{5} + 1)/2$  is the golden ratio and  $A(m) \equiv \int_0^{T/2} f_{\text{ellip}}(t; T, m, \theta = 0) dt$ . This gives  $m_e = 0.9830783\dots$

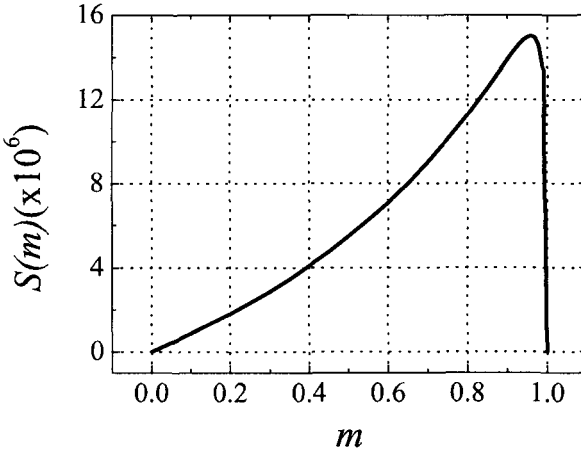


Figure 1.15: Shape function  $S(m)$  (Eq. (1.28)).

One finds that the degree of symmetry breaking mechanism confirms and explains all the previous experimental, theoretical, and numerical results from a great diversity of systems subjected to a biharmonic force (1.23). This is the case of the ac driven, damped sine-Gordon equation,

$$\phi_{tt} - \phi_{xx} + \sin(\phi) = -\beta\phi_t + f(t), \quad (1.29)$$

where directed energy transport requires a non-zero topological charge, implying the existence of sine-Gordon solitons (kinks) in the system. It is worth mentioning that

the sine-Gordon equation has important applications to superconducting devices such as long Josephson junctions. In the simple case of a biharmonic force,

$$f(t) = \epsilon_1 \sin(\delta t + \delta_0) + \epsilon_2 \sin(m\delta t + \delta_0 + \theta), \quad (1.30)$$

the kink velocity may be controlled by changing both the initial phase  $\delta_0$  and the relative phase  $\theta$  (with the remaining force parameters held constant). In the following, control of kink-mediated directed energy transport by using the elliptic force (1.26) is discussed. One firstly obtains the Fourier series of the force:

$$f_{\text{ellip}}(t) = \epsilon \sum_{n=1}^{\infty} a_n(m) \sin \left[ n \left( \frac{2\pi t}{T} + \theta \right) \right], \quad (1.31)$$

$$a_n(m) \equiv \frac{\pi^2 n}{mK^2(m)} \operatorname{sech} \left[ \frac{n\pi K(1-m)}{K(m)} \right]. \quad (1.32)$$

Now a collective coordinate approach with two degrees of freedom,  $X(t)$  and  $l(t)$  (respectively, position and width of the kink), can be directly applied to obtain the dynamics of these two collective coordinates in the presence of the elliptic force:

$$\begin{aligned} \dot{P} &= -\beta P - qf_{\text{ellip}}(t), \\ \ddot{l} &= \dot{l}^2/(2l) + 1/(2\alpha l) - \beta \dot{l} \\ &\quad - (\Omega_R^2 l/2) (1 + P^2/M_0^2), \end{aligned} \quad (1.33)$$

where the momentum  $P(t) = M_0 l_0 \dot{X}/l(t)$ ,  $\Omega_R = \sqrt{12}/(\pi l_0)$  is the Rice frequency,  $\alpha = \pi^2/12$ , and  $M_0 = 8$ ,  $q = 2\pi$ , and  $l_0 = 1$  are, respectively, the dimensionless kink mass, topological charge, and unperturbed width. From Eq. (1.31), one sees that, even for  $m$  values very close to 1, the force may be reliably approximated by its two first harmonics. For this biharmonic approximation, one straightforwardly obtains the following estimate for the average velocity of the kink,

$$\begin{aligned} \langle \dot{X}(t) \rangle &\equiv \frac{1}{T} \int_0^T \frac{P(t)l(t)}{M_0 l_0} dt = \langle \dot{X}_0(t) \rangle + \epsilon \langle \dot{X}_1(t) \rangle + \dots \\ &= F(\epsilon, \beta, T)S(m), \end{aligned} \quad (1.34)$$

with

$$\begin{aligned} F(\epsilon, \beta, T) &\equiv \frac{2q^3 \Omega_R^2 \epsilon^3 \pi^6}{M_0^4 (\beta^2 + 4\pi^2/T^2) (\beta^2 + 16\pi^2/T^2)^{1/2}} \\ &\quad \times \sum_{i=1}^2 \frac{2 \cos \left[ (\chi_2 - 2\chi_1) + (-1)^i \tilde{\theta}_i \right] (-1)^{i-1}}{i \sqrt{(\Omega_R^2 - 4i^2\pi^2/T^2)^2 + 4i^2\pi^2\beta^2/T^2}}, \end{aligned} \quad (1.35)$$

where

$$\begin{aligned}
 \chi_2 &= \arctan\left(\frac{4\pi}{\beta T}\right), \\
 \chi_1 &= \arctan\left(\frac{2\pi}{\beta T}\right), \\
 \tilde{\theta}_1 &= \arctan\left(\frac{T\Omega_R^2 - 4\pi^2/T}{2\pi\beta}\right), \\
 \tilde{\theta}_2 &= \arctan\left(\frac{T\Omega_R^2 - 16\pi^2/T}{4\pi\beta}\right),
 \end{aligned} \tag{1.36}$$

and where, as expected,  $\langle \dot{X}_0(t) \rangle = 0$ , and  $S(m)$  is the shape function (1.28). From Eqs. (1.34)-(1.36), one sees that the average velocity is *independent* of the initial phase  $\theta$ , while a *nonzero* velocity exists for  $0 < m < 1$  according to the degree of symmetry breaking mechanism.

#### 1.4.6 Reshaping-induced control of synchronization of coupled limit-cycle oscillators

As a seventh example, consider a system of  $N$  coupled oscillators with phases  $\phi_i \in [0, 2\pi]$ . In particular, the dynamics of the system is described by the following  $N$  differential-difference equations:

$$\frac{d\phi_i(t)}{dt} = \omega_0 + 2\epsilon \sum_j f_{\text{ellip}}[\phi_j(t - \tau) - \phi_i(t); T, m, \theta], \tag{1.37}$$

with  $T = 2\pi, \theta = 0$ , and where  $\epsilon$  is the coupling constant,  $\tau$  is the delay,  $\omega_0$  is the intrinsic frequency of the oscillators, and  $f_{\text{ellip}}(\cdot; T, m, \theta)$  if the elliptic force (1.31). It is straightforward to obtain that the lowest stable frequency associated with the synchronization states ( $\phi_i = \Omega t + \Phi_0$ ) for the biharmonic approximation corresponding to the elliptic coupling is given by

$$\Omega_{\min} \approx \frac{\omega_0}{1 + 2\pi^2 n \tau \epsilon g(m)}, \tag{1.38}$$

where  $n$  is the number of neighbours (four in the case of a square lattice with nearest-neighbour interaction) and

$$g(m) \equiv \frac{\text{sech}[\pi K(1 - m)/K(m)] + 4 \text{sech}[2\pi K(1 - m)/K(m)]}{mK^2(m)}. \tag{1.39}$$

Figure 1.16 shows the symmetry-breaking-induced frequency suppression ( $\Omega_{\min}/\omega_0$  versus  $m$ ) for the parameters  $n = 4, \tau = 0.1$ , and  $\epsilon = 3$ . Note that the minimum ( $m = 0.9845 \simeq m_e$ ) is the *same* for all values of  $\tau, n$ , and  $\epsilon$ .

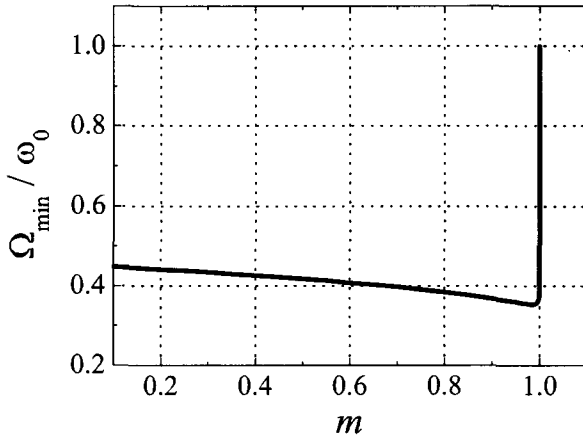


Figure 1.16: Lowest synchronization frequency vs shape parameter (Eq. (1.38)).

## 1.5 Notes and references

In this chapter the main features, advantages, and difficulties of two basic control approaches (feedback and non-feedback) were briefly discussed. A much more detailed description of a wide spectrum of such control methods, including classical control methods of engineering, can be found in Chen and Dong [1]. Although control of chaos represents nowadays one of the most active areas of research in the field of nonlinear dynamics, it is remarkable that classical control theory was originally developed for industrial and military applications [2]. For feedback methods, the interested reader is referred to Ref. [3].

At present, the literature concerning theoretical, numerical, and experimental studies of non-feedback methods is frankly unapproachable in a monograph of the present type. Therefore, only pioneering key work (from the author's viewpoint) is mentioned in the following. The effectiveness of periodic parametric excitations in suppressing chaos was shown by Alekseev and Loskutov in Ref. [4]. Hübler and Lüscher [5] discussed how a nonlinear oscillator can be driven towards a given target dynamics by means of resonant excitations. Braiman and Goldhirsch [6] provided numerical evidence to show the possibility of inhibiting chaos by an additional periodic external excitation. Salerno [7] showed the possibility of suppressing chaos in long biharmonically driven Josephson junctions by the analysis of a phase-locked map. Comments on references containing the application of Melnikov's method to the problem of control of chaos by small-amplitude harmonic excitations are included in the next chapter for the sake of completeness. Experimental control of chaos by

weak periodic excitations has been demonstrated in many diverse systems [11-24].

The ratchet effect [25] presents promising applications in a great diversity of problems, such as electronic transport through molecules [26], smoothing surfaces [27], controlling vortex density in superconductors [28], separating particles [29], controlling directed current in semiconductors [30], and rectifying the phase across a SQUID [31].

Synchronization phenomena are of great interest in diverse fields, such as science, engineering, and social life, where apparently different phenomena can be understood within a common framework. The synchronization of periodic oscillators, chaotic systems, large ensembles, and oscillatory media has attracted constant interest for many decades [32]. In particular, globally coupled oscillators are a simple class of many-body dynamical systems, in which each oscillator is coupled to all the others [33-35].

The discussion of many of the results of this chapter originated in work by the present author and coworkers [8-10,36].

- [1] Chen, G. and Dong, X., (1998) *From Chaos to Order: Perspectives, Methodologies and Applications*, World Scientific, Singapore.
- [2] Sontag, E. D., (1998) *Mathematical Control Theory: Deterministic Finite-Dimensional Systems*, Springer, Berlin, 2nd ed.
- [3] Ott, E., Sauer, T., and Yorke, J. A., (1994) *Coping with Chaos*, Chapter 12: "Control: Theory of Stabilization of Unstable Orbits," Wiley, New York.
- [4] Alekseev, V. V. and Loskutov, A. Y., (1987) "Control of a system with a strange attractor through periodic parametric action," *Sov. Phys. Dokl.* **32**, pp. 1346-1348.
- [5] Hübler, A. W. and Lüscher, E., (1989) "Resonant stimulation and control of nonlinear oscillators," *Naturwissenschaft* **76**, pp. 67-69.
- [6] Braiman, Y. and Goldhirsch, I., (1991) "Taming chaotic dynamics with weak periodic perturbations," *Phys. Rev. Lett.* **66**, pp. 2545-2548.
- [7] Salerno, M., (1991) "Suppression of phase-locking chaos in long Josephson junctions by biharmonic microwave fields," *Phys. Rev. B* **44**, pp. 2720-2726.
- [8] Chacón, R. and Díaz Bejarano, J., (1993) "Routes to suppressing chaos by weak periodic perturbations," *Phys. Rev. Lett.* **71**, pp. 3103-3106.
- [9] Chacón, R. and Martínez García-Hoz, A., (2002) "Route to chaos via strange non-chaotic attractors by reshaping periodic excitations," *Europhys. Lett.* **57** (1), pp. 7-13.
- [10] Chacón, R., (2002) "Modifying fractal basin boundaries by reshaping periodic terms," *J. Math. Phys.* **43** (7), pp. 3586-3591.
- [11] Ditto, W. L., Raueo, S. N., and Spano, M. L., (1990) "Experimental control of chaos," *Phys. Rev. Lett.* **65**, pp. 3211-3214.
- [12] Azevedo, A. and Rezende, S. M., (1991) "Controlling chaos in spin-wave instabilities," *Phys. Rev. Lett.* **66**, pp. 1342-1345.

- [13] Hunt, E. R., (1991) "Stabilizing high-period orbits in a chaotic system: The diode resonator," *Phys. Rev. Lett.* **68**, pp. 1953-1955.
- [14] Roy, R., Murphy, T. W., Maier, T. D., Gills, Z., and Hunt, E. R., (1992) "Dynamical control of a chaotic laser: Experimental stabilization of a globally coupled system," *Phys. Rev. Lett.* **68**, pp. 1259-1262.
- [15] Petrov, V., Gaspar, V., Masere, J., and Showalter, K., (1993) "Controlling chaos in the Belousov-Zhabotinsky reaction," *Nature (London)*, **361**, pp. 240-243.
- [16] Meucci, R., Gadomski, W., Ciofini, M., and Arcchi, F. T., (1994) "Experimental control of chaos by means of weak parametric perturbations," *Phys. Rev. E* **49**, pp. R2528-R2531.
- [17] Ding, W. X., She, H. Q., Huang, W., and Yu, C. X., (1994) "Controlling chaos in a discharge plasma," *Phys. Rev. Lett.* **72**, pp. 96-99.
- [18] Schiff, S. J. *et al.*, (1994) "Controlling chaos in the brain," *Nature* **370**, pp. 615-620.
- [19] Vohra, S. T., Fabiny, L., and Bucholtz, F., (1995) "Suppressed and induced chaos by near resonant perturbation of bifurcations," *Phys. Rev. Lett.* **75** (1), pp. 65-68.
- [20] Chizhevsky, V. N. and Corbalán, R., (1996) "Experimental observation of perturbation-induced intermittency in the dynamics of a loss-modulated CO<sub>2</sub> Laser," *Phys. Rev. E* **54** (5), pp. 4576-4579.
- [21] Dangoisse, D., Celet, J.-C., and Glorieux, P., (1997) "Global investigation of the influence of the phase of subharmonic excitation of a driven system," *Phys. Rev. E* **56** (2), pp. 1396-1406.
- [22] Uchida, A., Sato, T., Ogawa, T., and Kannari, F., (1998) "Nonfeedback control of chaos in a microchip solid-state laser by internal frequency resonance," *Phys. Rev. E* **58** (6), pp. 7249-7255.
- [23] Schwartz, I. B., Triandaf, I., Meucci, R., and Carr, T. W., (2002) "Open-loop sustained chaos and control: a manifold approach," *Phys. Rev. E* **66** (2), pp. 026213/1-7.
- [24] Alonso, S., Sagués, F., and Mikhailov, A. S., (2003) "Taming Winfree turbulence of scroll waves in excitable media," *Science* **299** (5607), pp. 1722-1725.
- [25] Reimann, P., (2002) "Brownian motors: noisy transport far from the equilibrium," *Phys. Rep.* **361**, pp. 57-265.
- [26] Lehmann, J., Kohler, S., Hänggi, P., and Nitzan, A., (2003) "Rectification of laser-induced electronic transport through molecules," *J. Chem. Phys.* **118**, pp. 3283-3292.
- [27] Derényi, I., Lee, C.-S., and Barabási, A.-L., (1998) "Ratchet effect in surface electromigration: smoothing surfaces by an AC field," *Phys. Rev. Lett.* **80**, pp. 1473-1476.
- [28] Lee, C.-S., Jankó, B., Derényi, I., and Barabási, A.-L., (1999) "Reducing vortex density in superconductors using the ratchet effect," *Nature* **400**, pp. 337-340.
- [29] Rousselet, J., Salome, L., Ajdari, A., and Prost, J., (1994) "Directional motion of Brownian particles induced by a periodic asymmetric potential," *Nature* **370**, pp. 446-448.

- [30] Alekseev, K. N., Erementchouk, M. V., and Kusmartsev, F. V., (1999) "Direct current generation due to wave mixing in semiconductors," *Europhys. Lett.* **47**, pp. 595-600.
- [31] Zapata, I., Bartussek, R., Sols, F., and Hänggi, P., (1996) "Voltage rectification by a SQUID ratchet," *Phys. Rev. Lett.* **77**, pp. 2292-2295.
- [32] Pikovsky, A. Rosenblum, M., and Kurths, J., (2001) *Synchronization. A universal concept in nonlinear sciences*, Cambridge University Press, Cambridge.
- [33] Niebur, E., Schuster, H. G., and Kammen, D. M., (1991) "Collective frequencies and metastability in networks of limit-cycle oscillators with time delay," *Phys. Rev. Lett.* **67**, pp. 2753-2756.
- [34] Strogatz, S. H., Mirollo, R. E., and Matthews, P. C., (1992) "Coupled nonlinear oscillators below the synchronization threshold: Relaxation by generalized Landau damping," *Phys. Rev. Lett.* **68**, pp. 2730-2733.
- [35] Zheng, Z., Hu, G., and Hu, B., (1998) "Phase slips and phase synchronization of coupled oscillators," *Phys. Rev. Lett.* **81**, pp. 5318-5321.
- [36] Chacón, R. and Quintero, N. R., (2005) "On the ratchet effect," *arXiv:physics/0503125* (preprint).